

3-D Vibration analysis of FG-MWCNTs/Phenolic sandwich sectorial plates

Vahid Tahouneh*

Young Researchers and Elite Club, Islamshahr Branch, Islamic Azad University, Islamshahr, Iran

(Received June 19, 2017, Revised December 1, 2017, Accepted December 27, 2017)

Abstract. In this study, based on the three-dimensional theory of elasticity, free vibration characteristics of sandwich sectorial plates with multiwalled carbon nanotube-(MWCNT)-reinforced composite core are considered. Modified Halpin-Tsai equation is used to evaluate the Young's modulus of the MWCNT/epoxy composite samples by the incorporation of an orientation as well as an exponential shape factor in the equation. The exponential shape factor modifies the Halpin-Tsai equation from expressing a straight line to a nonlinear one in the MWCNTs wt% range considered. In this paper, free vibration of thick functionally graded sandwich annular sectorial plates with simply supported radial edges and different circular edge conditions including simply supported-clamped, clamped-clamped, and free-clamped is investigated. A semi-analytical approach composed of two-dimensional differential quadrature method and series solution are adopted to solve the equations of motion. The material properties change continuously through the core thickness of the plate, which can vary according to a power-law, exponentially, or any other formulations in this direction. This study serves as a benchmark for assessing the validity of numerical methods or two-dimensional theories used to analysis of laminated sectorial plates.

Keywords: sandwich sectorial plates; vibration; modified Halpin-Tsai equation; three-dimensional theory of elasticity

1. Introduction

Nowadays, the use of carbon nanotubes in polymer/carbon nanotube composites has attracted wide attention (Wagner *et al.* 1997). A high aspect ratio, low weight of CNTs and their extraordinary mechanical properties (strength and flexibility) provide the ultimate reinforcement for the next generation of extremely lightweight but highly elastic and very strong advanced composite materials. On the other hand, by using of the polymer/CNT composites in advanced multilayered composite materials (sandwich structures) we can achieve structures with low weight, high strength and high stiffness in many structures of civil, mechanical and space engineering.

Functionally graded materials (FGMs) are heterogeneous materials in which the elastic and thermal properties change from one surface to the other, gradually and continuously. The material is constructed by smoothly changing the volume fraction of its constituent materials. FGMs offer great promise in applications where the operating conditions are severe, including spacecraft heat shields, heat exchanger tubes, plasma facings for fusion reactors, engine components, and high-power electrical contacts or even magnets. For example, in a conventional thermal barrier coating for high-temperature applications, a discrete layer of ceramic material is bonded to a metallic structure. However, the abrupt transition in material

properties across the interface between distinct materials can cause large interlaminar stresses and lead to plastic deformation or cracking (Finot and Suresh 1996). These adverse effects can be alleviated by functionally grading the material to have a smooth spatial variation of material composition. The concept of FGMs was first introduced in Japan in 1984. Since then it has gained considerable attention (Koizumi 1993). A lot of different applications of FGMs can be found in (Zhu and Meng 1995). Ramakris and Kunukkas (1973) provided a closed-form analytical solution for free vibration of an annular sector plate with radial edges simply supported. Mukhopadhyay (1979 and 1982) used a semi-analytical method and Srinivasan and Thiruvengkatachari (1983 and 1986) used the integral equation technique to analyze the vibrations of annular sector plates, respectively. Kim and Dickinson (1989) used one-dimensional (1-D) orthogonal polynomials and Liew and Lam (1993) used two-dimensional (2-D) orthogonal polynomials as admissible functions to study the free vibration of annular sector plates by the Rayleigh-Ritz method. Ramaiah and Vijayakumar (1974) studied the free vibration of annular sector plates with simply supported radial edges by a combination of the Rayleigh-Ritz method and coordinate transformation. Swaminadham *et al.* (1984) compared the natural frequencies of annular sector plates from the finite element method and experiments. Seok and Tiersten (2004) used a variational approximation procedure to analyze the free vibration of cantilevered annular sector plates. Houmat (2001) used the hierarchical finite element method to study the free vibration of annular sector plates. The Lagrange identity method was developed by Marin (1994) for the study of the initial boundary value problem of thermoelasticity of bodies with microstructure. This researcher outlined some estimations on the basis that some

*Corresponding author, Ph.D.,
E-mail: vahid.th1982@gmail.com;
vahid.tahouneh@ut.ac.ir

uniqueness and continuous dependence theorems in bounded and exterior domains could be obtained. Sharma and Marin (2013) considered wave propagation in micropolar thermoelastic solid half space with distinct conductive and thermodynamic temperatures. Reflection of plane waves incident obliquely at the free surface of micropolar generalized thermoelastic solid half space. Marin (2010a) extended the concept of domain of influence in order to cover the elasticity of microstretch materials. Marin (1997) considered the general results from the theory of elliptic equations were applied in order to obtain the existence and uniqueness of the generalized solutions for the boundary value problems in elasticity of dipolar materials with voids. Marin (2010b) studied a cylinder made of a microstretch thermoelastic material for which one plane end was subjected to plane boundary data varying harmonically in time. Results showed that the amplitude of the vibrations decays exponentially with the distance to the base. Sharma *et al.* (2005a, b) integrated an analytical approach with the Chebyshev polynomials technique to study the buckling and free vibration of isotropic and laminated composite sector plates based on the first-order shear deformation theory. For moderate thickness plates, the first-order shear deformable plate theory is commonly used, which could provide a result more accurate than that from the CPT. Liew and Liu (2000) used the differential quadrature method to analyze the free vibration of thick annular sector plates. Wu and Liu (2016) developed a state space differential reproducing kernel (DRK) method in order to study 3D analysis of FG circular plates. Park *et al.* (2016) used modified couple stress based third-order shear deformation theory for dynamic analysis of sigmoid functionally graded materials (S-FGM) plates. Bapu Rao *et al.* (1977) and Guruswamy and Yang (1979) used the finite element method to analyze the vibrations of thick annular sector plates. Benson and Hinton (1976) and Cheung and Chan (1981) used the finite strip method to carry out static and dynamic analyses of thick annular sector plates. Mizusawa (1991) used the finite element method to study the natural frequencies of thick annular sector plates. Xiang *et al.* (1993) applied the Ritz method to study the free vibration of thick annular sector plates. Leissa *et al.* (Leissa *et al.* 1993 and McGee *et al.* 1995) considered the effect of stress singularities on the vibration analysis of thick annular sector plates and presented the corner functions to improve the convergence of the numerical solutions. Zhou *et al.* (2009) used the Chebyshev-Ritz method to study the free vibration of thick annular sector plates, Nie and Zhong (2008) investigated the free and forced vibration analysis of FGM annular sector plates with simply-supported radial edges by using a semi-analytical approach. Arefi (2015) suggested an analytical solution of a curved beam with different shapes made of functionally graded materials (FGMs). Bennai *et al.* (2015) developed a new refined hyperbolic shear and normal deformation beam theory to study the free vibration and buckling of functionally graded (FG) sandwich beams under various boundary conditions. Bouchafa *et al.* (2015) used refined hyperbolic shear deformation theory (RHSDT) for the thermoelastic bending analysis of functionally graded sandwich plates.

Bouguenina *et al.* (2015) studied FG plates with variable thickness subjected to thermal buckling. Tahouneh (2016) presented a 3-D elasticity solution for free vibration analysis of continuously graded carbon nanotube-reinforced (CGCNT) rectangular plates resting on two-parameter elastic foundations. The volume fractions of oriented, straight single-walled carbon nanotubes (SWCNTs) were assumed to be graded in the thickness direction. Moradi-Dastjerdi and Momeni-Khabisi (2016) studied Free and forced vibration of plates reinforced by wavy carbon nanotube (CNT). The plates were resting on Winkler-Pasternak elastic foundation and subjected to periodic or impact loading. Nowadays, the use of carbon nanotubes in polymer/carbon nanotube composites has attracted wide attention (Wagner *et al.* 1997). A high aspect ratio, low weight of CNTs and their extraordinary mechanical properties (strength and flexibility) provide the ultimate reinforcement for the next generation of extremely lightweight but highly elastic and very strong advanced composite materials. On the other hand, by using of the polymer/CNT composites in advanced composite materials, we can achieve structures with low weight, high strength and high stiffness in many structures of civil, mechanical and space engineering.

Several researches have recently investigated the elastic properties of multiwalled carbon nanotube (MWCNT) and their composites (Fidelus *et al.* 2005, Ghavamian *et al.* 2012). Gojny *et al.* (2005) focused on the evaluation of the different types of the CNTs applied, their influence on the mechanical properties of epoxy-based nanocomposites and the relevance of surface functionalization. Therefore, the study of the mechanical performance of CNT-based composites and the discovery of possible innovative applications has recently attracted the interest of many researchers.

Several researchers have reported that mechanical properties of polymeric matrices can be drastically increased (Montazeri *et al.* 2010, Yeh *et al.* 2006) by adding a few weight percent (wt%) MWCNTs. Montazeri *et al.* (2010) showed that modified Halpin-Tsai equation with exponential Aspect ratio can be used to model the experimental result of MWNT composite samples. They also demonstrated that reduction in Aspect ratio (L/d) and nanotube length cause a decrease in aggregation and Above 1.5wt%, nanotubes agglomerate causing a reduction in Young's modulus values. Thus, it is important to determine the effect Aspect ratio and arrangement of CNTs on the effective properties of carbon nanotube-reinforced composite (CNTRC). Yeh *et al.* (2006) used the Halpin-Tsai equation to shows the effect of MWNT shape factor (L/d) on the mechanical properties. They showed that the mechanical properties of nanocomposite samples with the higher shape factor (L/d) values were better than the ones with the lower shape factor. The reinforcement effect of MWCNTs with different aspect ratio in an epoxy matrix has been carried out by Martone *et al.* (2011). They showed that progressive reduction of the tubes effective aspect ratio occurs because of the increasing connectedness between tubes upon an increase in their concentration. Also they investigated on the effect of nanotube curvature on the

average contacts number between tubes by means of the waviness that accounts for the deviation from the straight particles assumption. Though there are research works reported on general sandwich structures, very little work has been done to consider even the vibration behavior of FG sandwich structures (Anderson 2003, Kashtalyan and Menshykova 2009, Barka *et al.* 2016, Chen *et al.* 2017). Li *et al.* (2008) studied free vibrations of FGSW rectangular plates with simply supported and clamped edges. Zenkour (2005a, b) presented a two-dimensional solution to study the bending, buckling and free vibration of simply supported FG ceramic-metal sandwich plates. Kamarian *et al.* (2013) studied free vibration of FGSW rectangular plates with simply supported edges and rested on elastic foundations using differential quadratic method. Very recently, Wang and Shen (2011) investigated the large amplitude vibration and the nonlinear bending of a sandwich plate with CNTRC face sheets resting on an elastic foundation on the basis of a micromechanical model and multi-scale approach. Tahouneh and Naei (2015) investigated free vibration and vibrational displacements of thick laminated curved panels with finite via DQ method. The material properties varied continuously through the layers' thickness according to a three-parameter power-law distribution. It was assumed that the inner surfaces of the functionally graded sheets are metal rich, while the outer surfaces of the layers could be metal rich, ceramic rich or made of a mixture of two constituents.

To the author's best knowledge, there is not any work about vibrational analysis of FG-MWCNT sandwich structures. The aim of this study is to fill this apparent gap in this area by providing the 3-D vibration analysis results for FG-MWCNT sandwich sectorial plates with power-law distribution of multiwalled carbon nano tubes. The effective material properties of the FG-MWCNT plates are estimated using a modified Halpin-Tsai equation. Also a parametric study is carried out to highlight the influence of MWCNT volume fraction in the structure thickness, type of CNT distributions and geometrical parameters on vibration behavior of FG- MWCNT sandwich sectorial plates.

2. Problem description

2.1 Mechanical properties of the structure

Consider a sandwich annular sector plate as shown in Fig. 1. This plate is referring to a cylindrical coordinate system (r, θ, z) , as depicted in this figure. It is assumed the

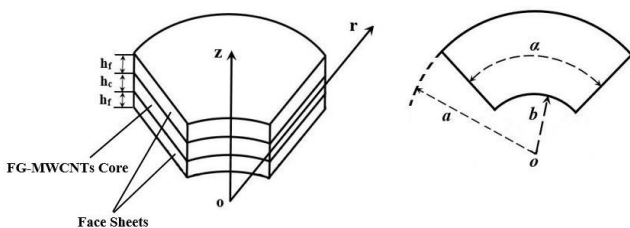


Fig. 1 An annular sandwich sector plate with radial edges simply supported

total thickness of structure is “ h ”. The structure has continuous grading of reinforcement through thickness direction. In this study, we will discuss about the results in the literature on mechanical properties of polymer nanotube composites. The Halpin-Tsai equation assumes that the filler are straight and uniform dispersion of the filler in the polymer matrix. The Halpin-Tsai equation (Halpin and Tsai 1969, Affdl Halpin and Kardos 1976) has been recognized for its ability to predict the modulus values for the fiber-reinforced composite samples. The effective mechanical properties of the CNTRC plate are obtained based on a modified Halpin-Tsai equation according to (Montazeri *et al.* 2010, Yeh *et al.* 2006)

$$E = E_m \frac{1 + \eta_L \eta_T V_{cn}}{1 - \eta_T V_{cn}}, \eta_T = \frac{\alpha E_{cn} / E_m - 1}{\alpha E_{cn} / E_m + \eta_L} \quad (1)$$

The effective Young's modulus of MWCNT can be deduced from Eq. (1) as follows

$$E_f = \frac{(2l/d + V_{cn})E - 2l/d(1 - V_{cn})E_m}{\alpha[(2l/d + V_{cn} + 1)E_m - (1 - V_{cn})E]} E_m \quad (2)$$

From the linear region of the fitting line for MWNTs/phenolic composites, the effective Young's modulus (E_f) of MWNT is 953 GPa. In above equations, E_{cn} and E_m are the longitudinal elastic moduli of the MWCNT and pure polymer; V_{cn} is the CNT volume fraction; η_L is the exponential shape factor; l and d are the length and the diameter of CNT and α is CNT orientation efficiency.

$$\eta_L = 2 \frac{l}{d} e^{-aV_{cn} - b} \quad (3)$$

In which η_L is related to the aspect ratio of reinforcement length l and diameter d in the Halpin-Tsai equation. a and b are constants, related to the degree of MWCNTs aggregation, which account for the nonlinear behavior of the Halpin-Tsai equation in the MWCNTs wt% range considered (Montazeri *et al.* 2010, Yeh *et al.* 2006). The resulting effective properties for the randomly oriented MWCNT composite are isotropic, despite the CNTs having transversely isotropic effective properties. The orientation of a straight CNT is characterized by α .

When CNTs are completely randomly oriented in the matrix, the composite is then isotropic. In this article, the experimental data for the Young's modulus of MWCNT/phenolic composites with different mass fraction of MWCNTs, reported by Yeh *et al.* (2006), was used to fit the above Halpin-Tsai equation. In Fig. 2, the predicted Young's moduli using Eq. (1) is shown.

The best fit was achieved by taking the model

Table 1 Material properties for the pure phenolic the MWCNTs

Polymer (phenolic)	MWCNTs
$E_m = 5.13 \text{ GPa}$	$E_{cn} = 953 \text{ GPa}, \rho_{cn} = 1.30 \text{ g/ml}, v_{cn} = 0.29$
$\rho_m = 1.03 \text{ g/ml}$	$\alpha = 1/6, l = 17.57 \mu\text{m}, d = 23.63 \text{ nm},$
$v_m = 0.34$	$a = 75, b = 1$

parameters given in Table 1. Using this prediction model, the Young's modulus of functionally graded MWCNT/phenolic composites will be estimated during the numerical solutions in the next sections. Also, the mass density and Poisson's ratio of the MWCNT/phenolic composite according to rule of mixtures can be calculated, respectively, by

$$v_{ij} = V_{cn} v^{cn} + V_m v^m, \quad ij = 12, 13 \text{ and } 23 \tag{4}$$

$$\rho = V_{cn} \rho^{cn} + V_m \rho^m$$

where v^{cn} and ρ^{cn} are Poisson's ratio and density, respectively, of the CNT and v^m and ρ^m are corresponding properties for the matrix. The reinforcement volume fraction of FG-MWCNT panel is assumed as follows (Pelletier Jacob and VelSenthil 2006)

$$V_{MWCNT} = \begin{cases} V_i, & -0.5h_c \leq z \leq -0.5h_c \\ V_i + (V_o - V_i) \left(\frac{z + 0.5h_c}{h_c} \right)^p, & -0.5h_c \leq z \leq 0.5h_c \\ V_o, & 0.5h_c \leq z \leq 0.5h_c \end{cases} \tag{5}$$

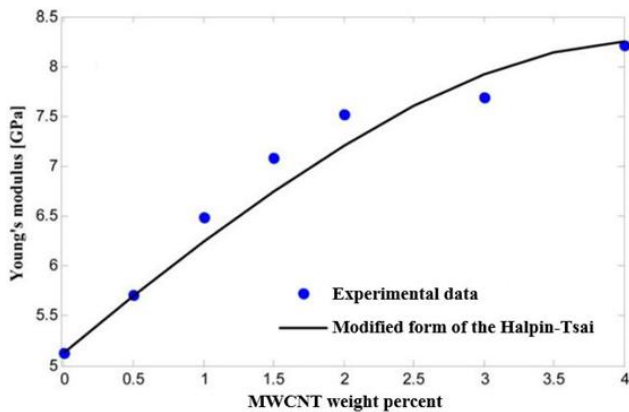


Fig. 2 Prediction of the Young's modulus of MWCNT/phenolic composites containing various wt% of MWCNTs (Yeh *et al.* 2006)

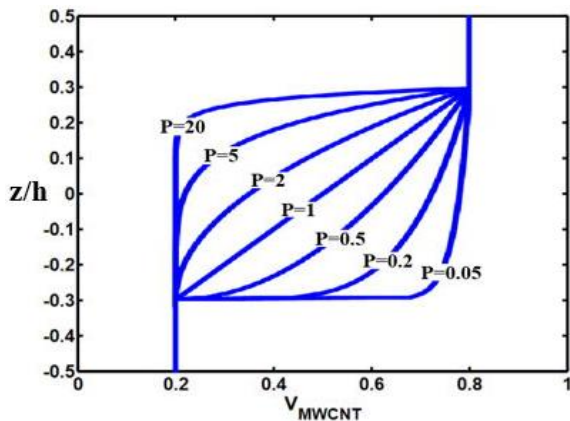


Fig. 3 Variations of the volume fraction of reinforcement (V_{MWCNT}) through the thickness direction of sandwich sectorial plates for different values of "p"

where V_i and V_o , which have values that range from 0 to 1. The exponent "p" governs the through-thickness fiber volume fraction profile. The through-thickness variations of the volume fractions are depicted in Fig. 3. As shown in Fig. 3, the volume fraction of core varies from 0.2 to 0.8 as η ($\eta = z/h$) varies from $-h_c/2$ and $h_c/2$ while the reinforcement volume fractions of top and bottom faces are 0.8 and 0.2, respectively.

3. Governing equations

In the absence of body forces, the governing equations are as follows (Reddy 2013)

$$\frac{\partial \sigma_r}{\partial r} + \frac{1}{r} \frac{\partial \tau_{r\theta}}{\partial \theta} + \frac{\partial \tau_{rz}}{\partial z} + \frac{\sigma_r - \sigma_\theta}{r} = \rho \frac{\partial^2 u_r}{\partial t^2}$$

$$\frac{\partial \tau_{r\theta}}{\partial r} + \frac{1}{r} \frac{\partial \sigma_\theta}{\partial \theta} + \frac{\partial \tau_{\theta z}}{\partial z} + \frac{2\tau_{r\theta}}{r} = \rho \frac{\partial^2 u_\theta}{\partial t^2} \tag{6}$$

$$\frac{\partial \tau_{rz}}{\partial r} + \frac{1}{r} \frac{\partial \tau_{\theta z}}{\partial \theta} + \frac{\partial \sigma_z}{\partial z} + \frac{\tau_{rz}}{r} = \rho \frac{\partial^2 u_z}{\partial t^2}$$

Where $\sigma_r, \sigma_\theta, \sigma_z$ are axial stress components, $\tau_{r\theta}, \tau_{\theta z}, \tau_{rz}$ are shear stress components, u_r, u_θ, u_z are displacement components, ρ denotes material density and t is time. The relations between the strain and the displacement are

$$\epsilon_r = \frac{\partial u_r}{\partial r}, \epsilon_\theta = \frac{u_r}{r} + \frac{1}{r} \frac{\partial u_\theta}{\partial \theta}, \epsilon_z = \frac{\partial u_z}{\partial z},$$

$$\gamma_{\theta z} = \frac{\partial u_\theta}{\partial z} + \frac{1}{r} \frac{\partial u_z}{\partial \theta}, \gamma_{rz} = \frac{\partial u_r}{\partial z} + \frac{\partial u_z}{\partial r}, \tag{7}$$

$$\gamma_{r\theta} = \frac{1}{r} \frac{\partial u_r}{\partial \theta} + \frac{\partial u_\theta}{\partial r} - \frac{u_\theta}{r}$$

where $\epsilon_r, \epsilon_\theta, \epsilon_z, \gamma_{\theta z}, \gamma_{r\theta}, \gamma_{rz}$ are strain components. The constitutive equations for material are

$$\begin{Bmatrix} \sigma_r \\ \sigma_\theta \\ \sigma_z \\ \tau_{z\theta} \\ \tau_{rz} \\ \tau_{r\theta} \end{Bmatrix} = \begin{bmatrix} c_{11} & c_{12} & c_{13} & 0 & 0 & 0 \\ c_{12} & c_{22} & c_{23} & 0 & 0 & 0 \\ c_{13} & c_{23} & c_{33} & 0 & 0 & 0 \\ 0 & 0 & 0 & c_{44} & 0 & 0 \\ 0 & 0 & 0 & 0 & c_{55} & 0 \\ 0 & 0 & 0 & 0 & 0 & c_{66} \end{bmatrix} \begin{Bmatrix} \epsilon_r \\ \epsilon_\theta \\ \epsilon_z \\ \gamma_{z\theta} \\ \gamma_{rz} \\ \gamma_{r\theta} \end{Bmatrix} \tag{8}$$

In Eq. (8), c_{ij} are material elastic stiffness coefficients. Using the three-dimensional constitutive relations and the strain-displacement relations, the equations of motion in terms of displacement components for a linear elastic FG plate with infinitesimal deformations can be written as

-In the r direction

$$c_{11} \frac{\partial^2 u_r}{\partial r^2} + c_{12} \left(-\frac{1}{r^2} \frac{\partial u_\theta}{\partial \theta} + \frac{1}{r} \frac{\partial^2 u_\theta}{\partial r \partial \theta} + \frac{1}{r} \frac{\partial u_r}{\partial r} - \frac{1}{r^2} u_r \right)$$

$$+ c_{13} \frac{\partial^2 u_z}{\partial r \partial z} + \frac{c_{66}}{r} \left(\frac{\partial^2 u_\theta}{\partial \theta \partial r} + \frac{1}{r} \frac{\partial^2 u_r}{\partial \theta^2} - \frac{1}{r} \frac{\partial u_\theta}{\partial \theta} \right) \tag{9}$$

$$\begin{aligned}
 & c'_{55} \left(\frac{\partial u_r}{\partial z} + \frac{\partial u_z}{\partial r} \right) + c_{55} \left(\frac{\partial^2 u_r}{\partial z^2} + \frac{\partial^2 u_z}{\partial z \partial r} \right) \\
 & + \frac{1}{r} \left[c_{11} \frac{\partial u_r}{\partial r} + c_{12} \left(\frac{1}{r} \frac{\partial u_\theta}{\partial \theta} + \frac{u_r}{r} \right) + c_{13} \frac{\partial u_z}{\partial z} \right. \\
 & \left. - c_{12} \frac{\partial u_r}{\partial r} - c_{22} \left(\frac{1}{r} \frac{\partial u_\theta}{\partial \theta} + \frac{u_r}{r} \right) - c_{23} \frac{\partial u_z}{\partial z} \right] = \rho \frac{\partial^2 u_r}{\partial t^2}
 \end{aligned} \tag{9}$$

-In the θ direction

$$\begin{aligned}
 & c_{66} \left(\frac{\partial^2 u_\theta}{\partial r^2} - \frac{1}{r^2} \frac{\partial u_r}{\partial \theta} + \frac{1}{r} \frac{\partial^2 u_r}{\partial r \partial \theta} + \frac{1}{r^2} u_\theta - \frac{1}{r} \frac{\partial u_\theta}{\partial r} \right) \\
 & + \frac{1}{r} \left[c_{12} \frac{\partial^2 u_r}{\partial \theta \partial r} + c_{22} \left(\frac{1}{r} \frac{\partial^2 u_\theta}{\partial \theta^2} + \frac{1}{r} \frac{\partial u_r}{\partial \theta} \right) + c_{23} \frac{\partial^2 u_z}{\partial \theta \partial z} \right] \\
 & + c'_{44} \left(\frac{1}{r} \frac{\partial u_z}{\partial \theta} + \frac{\partial u_\theta}{\partial z} \right) + c_{44} \left(\frac{1}{r} \frac{\partial^2 u_z}{\partial z \partial \theta} + \frac{\partial^2 u_\theta}{\partial z^2} \right) \\
 & + \frac{2c_{66}}{r} \left(\frac{\partial u_\theta}{\partial r} + \frac{1}{r} \frac{\partial u_r}{\partial \theta} - \frac{u_\theta}{r} \right) = \rho \frac{\partial^2 u_\theta}{\partial t^2}
 \end{aligned} \tag{10}$$

-In the z direction

$$\begin{aligned}
 & c_{55} \left(\frac{\partial^2 u_r}{\partial r \partial z} + \frac{\partial^2 u_z}{\partial r^2} \right) + \frac{c_{44}}{r} \left(\frac{1}{r} \frac{\partial^2 u_z}{\partial \theta^2} + \frac{\partial^2 u_\theta}{\partial \theta \partial z} \right) \\
 & + c'_{13} \frac{\partial u_r}{\partial r} + c_{13} \frac{\partial^2 u_r}{\partial z \partial r} + c'_{23} \left(\frac{1}{r} \frac{\partial u_\theta}{\partial \theta} + \frac{u_r}{r} \right) \\
 & + c_{23} \left(\frac{1}{r} \frac{\partial^2 u_\theta}{\partial z \partial \theta} + \frac{1}{r} \frac{\partial u_r}{\partial z} \right) + c'_{33} \frac{\partial u_z}{\partial z} + c_{33} \frac{\partial^2 u_z}{\partial z^2} \\
 & + \frac{c_{55}}{r} \left(\frac{\partial u_r}{\partial z} + \frac{\partial u_z}{\partial r} \right) = \rho \frac{\partial^2 u_z}{\partial t^2}
 \end{aligned} \tag{11}$$

where $c'_{ij} = \frac{dc_{ij}}{dz}$.

Eqs. (9) and (10) represent the in-plane equations of motion along the r and θ -axes, respectively; and Eq. (11) is the transverse or out-of-plane equation of motion.

The related boundary conditions are as follows: at $z = -0.5 h$ and $0.5 h$

$$\tau_{zr} = 0, \tau_{z\theta} = 0, \sigma_z = 0 \tag{12}$$

In this paper three different kinds of boundary conditions are considered for circular edges including clamped-clamped (c-c), simply supported-clamped (s-c) and free-clamped (f-c). The boundary conditions at edges are

Clamped ($r = b$) – Clamped ($r = a$)

$$\begin{aligned}
 & \text{at } r = a \quad u_r = u_\theta = u_z = 0 \\
 & \text{at } r = b \quad u_r = u_\theta = u_z = 0
 \end{aligned} \tag{13}$$

Simply supported ($r = b$) – Clamped ($r = a$)

$$\begin{aligned}
 & \text{at } r = b \quad u_\theta = u_z = \sigma_r = 0 \\
 & \text{at } r = a \quad u_r = u_\theta = u_z = 0
 \end{aligned} \tag{14}$$

Free ($r = b$) – Clamped ($r = a$)

$$\begin{aligned}
 & \text{at } r = a \quad u_r = u_\theta = u_z = 0 \\
 & \text{at } r = b \quad \sigma_r = \tau_{r\theta} = \tau_{rz} = 0
 \end{aligned} \tag{15}$$

4. Solution procedure

Using the geometrical periodicity of the plate, the displacement components for the free vibration analysis can be represented as

$$\begin{aligned}
 U_r(r, \theta, z, t) &= U_{rm}(r, z) \sin(m\pi\theta/\alpha) e^{i\omega t}, \\
 U_\theta(r, \theta, z, t) &= U_{\theta m}(r, z) \cos(m\pi\theta/\alpha) e^{i\omega t}, \\
 U_z(r, \theta, z, t) &= U_{zm}(r, z) \sin(m\pi\theta/\alpha) e^{i\omega t}
 \end{aligned} \tag{16}$$

where $m (= 0, 1, \dots, \infty)$ is the circumferential wave number; ω is the natural frequency and $i (= \sqrt{-1})$ is the imaginary number. It is obvious that $m = 0$ means axisymmetric vibration. At this stage the GDQ [A brief review of GDQ method is given in Appendix] rules are employed to discretize the free vibration equations and the related boundary conditions. Substituting for the displacement components from (16) and then using the GDQ rules for the spatial derivatives, the discretized form of the equations of motion at each domain grid point (r_j, z_k) with ($j = 2, 3, \dots, N_r - 1$) and ($k = 2, 3, \dots, N_z - 1$) can be obtained as

Eq. (9)

$$\begin{aligned}
 & (c_{11})_k \sum_{n=1}^{N_r} B_{jn}^r u_{rmnk} + (c_{12})_k \left(\frac{m\pi}{r_j^2 \alpha} u_{\theta mjk} - \frac{m\pi}{r_j \alpha} \right. \\
 & \left. \sum_{n=1}^{N_r} A_{jn}^r u_{\theta mnk} + \frac{1}{r_j} \sum_{n=1}^{N_r} A_{jn}^r u_{rmnk} - \frac{1}{r_j} u_{rmjk} \right) \\
 & + (c_{13})_k \sum_{n=1}^{N_r} \sum_{r=1}^{N_z} A_{jn}^r A_{kr}^z u_{zmnr} + \frac{(c_{66})_k}{r_j} \left(-\frac{m\pi}{\alpha} \sum_{n=1}^{N_r} A_{jn}^r u_{\theta mnk} \right. \\
 & \left. - \frac{m^2 \pi^2}{r_j \alpha^2} u_{rmjk} + \frac{m\pi}{r_j \alpha} u_{\theta mjk} \right) + (c'_{55})_k \\
 & \left(\sum_{n=1}^{N_z} A_{kn}^z u_{rmjn} + \sum_{n=1}^{N_r} A_{jn}^r u_{zmnk} \right) \\
 & + (c_{55})_k \left(\sum_{n=1}^{N_z} B_{kn}^z u_{rmjn} + \sum_{n=1}^{N_r} \sum_{r=1}^{N_z} A_{jn}^r A_{kr}^z u_{zmnr} \right) \\
 & + \frac{1}{r_j} \left((c_{11})_k \sum_{n=1}^{N_r} A_{jn}^r u_{rmnk} + (c_{12})_k \left(\frac{m\pi}{r_j \alpha} u_{\theta mjk} + \frac{1}{r_j} u_{rmjk} \right) \right) \\
 & + (c_{13})_k \sum_{n=1}^{N_z} A_{kn}^z u_{zmn} - (c_{12})_k \sum_{n=1}^{N_r} A_{jn}^r u_{rmnk} \\
 & - (c_{22})_k \left(-\frac{m\pi}{r_j \alpha} u_{\theta mjk} + \frac{1}{r_j} u_{rmjk} \right) - (c_{23})_k \sum_{n=1}^{N_z} A_{kn}^z u_{zmn} \\
 & = -\rho_k \omega^2 u_{rmjk}
 \end{aligned} \tag{17}$$

Eq. (10)

$$(c_{66})_k \left(\sum_{n=1}^{N_r} B_{jn}^r u_{\theta mnk} - \frac{m\pi}{r_j^2 \alpha} u_{rmjk} + \frac{m\pi}{r_j \alpha} \sum_{n=1}^{N_r} A_{jn}^r u_{rmnk} \right) \tag{18}$$

$$\begin{aligned}
 & + \frac{1}{r_j^2} u_{\theta mjk} - \frac{1}{r_j} \sum_{n=1}^{N_r} A_{jn}^r u_{\theta mnk} + \frac{1}{r_j} ((c_{12})_k \left(\frac{m\pi}{\alpha} \sum_{n=1}^{N_r} A_{jn}^r u_{r mnk} \right. \\
 & + (c_{22})_k \left(-\frac{m^2 \pi^2}{r_j \alpha^2} u_{\theta mjk} + \frac{m\pi}{r_j \alpha} u_{r mj k} \right) + (c_{23})_k \left(\frac{m\pi}{\alpha} \sum_{n=1}^{N_z} A_{kn}^z u_{z mj n} \right. \\
 & \left. + (c'_{44})_k \left(\frac{m\pi}{r_j \alpha} u_{z mj k} + \sum_{n=1}^{N_z} A_{kn}^z u_{\theta mj n} \right) \right) \\
 & + (c_{44})_k \left(\frac{m\pi}{r_j \alpha} \sum_{n=1}^{N_z} A_{kn}^z u_{z mj n} + \sum_{n=1}^{N_z} B_{kn}^z u_{\theta mj n} \right) + \frac{2(c_{66})_k}{r_j} \\
 & \left(\sum_{n=1}^{N_r} A_{jn}^r u_{\theta mnk} + \frac{m\pi}{r_j \alpha} u_{r mj k} - \frac{u_{\theta mjk}}{r_j} \right) \\
 & = -\rho_k \omega^2 u_{\theta mjk}
 \end{aligned}
 \tag{18}$$

Eq. (11)

$$\begin{aligned}
 & (c_{55})_k \left(\sum_{n=1}^{N_r} \sum_{r=1}^{N_z} A_{kr}^z A_{jn}^r u_{r mn r} + \sum_{n=1}^{N_r} B_{jn}^r u_{z mnk} \right) \\
 & + \frac{(c_{44})_k}{r_j} \left(-\frac{m^2 \pi^2}{r_j \alpha^2} u_{z mj k} - \frac{m\pi}{\alpha} \sum_{n=1}^{N_z} A_{kn}^z u_{\theta mj n} \right) \\
 & + (c'_{13})_k \sum_{n=1}^{N_z} A_{kn}^z u_{r mj n} + (c_{13})_k \sum_{n=1}^{N_r} \sum_{r=1}^{N_z} A_{kr}^z A_{jn}^r u_{r mn r} \\
 & + (c'_{23})_k \left(-\frac{m\pi}{r_j \alpha} u_{\theta mjk} + \frac{u_{r mj k}}{r_j} \right) + (c_{23})_k \\
 & \left(-\frac{m\pi}{r_j \alpha} \sum_{n=1}^{N_z} A_{kn}^z u_{\theta mj n} + \frac{1}{r_j} \sum_{n=1}^{N_z} A_{kn}^z u_{r mj n} \right) + (c'_{33})_k \sum_{n=1}^{N_z} A_{kn}^z u_{z mj n} \\
 & + (c_{33})_k \sum_{n=1}^{N_z} B_{kn}^z u_{z mj n} + \frac{(c_{55})_k}{r_j} \left(\sum_{n=1}^{N_z} A_{kn}^z u_{r mj n} \right. \\
 & \left. + \sum_{r=1}^{N_r} A_{jr}^r u_{z mr k} \right) = -\rho_k \omega^2 u_{z mj k}
 \end{aligned}
 \tag{19}$$

where A_{ij}^r , A_{ij}^z and B_{ij}^r, B_{ij}^z are the first and second order GDQ weighting coefficients in the r - and z - directions, respectively.

In a similar manner the boundary conditions can be discretized. For this purpose, using Eq. (16) and then GDQ discretization rules for spatial derivatives, the boundary conditions at $z = -0.5 h$ and $0.5 h$ become,

Eq. (12)

$$\begin{aligned}
 & \sum_{n=1}^{N_z} A_{kn}^z u_{r mj n} + \sum_{n=1}^{N_r} A_{jn}^r u_{z mnk} = 0, \\
 & \frac{m\pi}{r_j \alpha} u_{z mj k} + \sum_{n=1}^{N_z} A_{kn}^z u_{\theta mj n} = 0, \\
 & (c_{13})_k \left(\sum_{n=1}^{N_r} A_{jn}^r u_{r mnk} \right) + (c_{23})_k \left(-\frac{m\pi}{r_j \alpha} u_{\theta mjk} + \frac{1}{r_j} u_{r mj k} \right) \\
 & + (c_{33})_k \left(\sum_{n=1}^{N_z} A_{kn}^z u_{z mj n} \right) = 0
 \end{aligned}
 \tag{20}$$

Table 2 Comparison of fundamental frequency parameter ($\Omega = \omega \alpha^2 \sqrt{\rho h/D}$) for flexural vibration of annular sector plates with two straight edges simply supported for $b/a = 0.5$

α (deg)	h/a	Theories	C-C	F-C	F-S	
0.01	0.1	McGee <i>et al.</i> (1995)	90.0837	21.4263	10.8761	
		Zhou <i>et al.</i> (2009)	90.1125	21.4074	10.8522	
		Present ($N_r = N_z = 9$)	90.1102	21.4065	10.8513	
		Present ($N_r = N_z = 13$)	90.1124	21.4075	10.8520	
		Present ($N_r = N_z = 17$)	90.1122	21.4076	10.8525	
		Present ($N_r = N_z = 19$)	90.1123	21.4076	10.8524	
	195	0.2	McGee <i>et al.</i> (1995)	70.8090	19.9986	10.2268
			Zhou <i>et al.</i> (2009)	71.9146	20.0967	10.2386
			Present ($N_r = N_z = 9$)	71.9115	20.0954	10.2392
			Present ($N_r = N_z = 13$)	71.9142	20.0964	10.2380
			Present ($N_r = N_z = 17$)	71.9143	20.0968	10.2385
			Present ($N_r = N_z = 19$)	71.9143	20.0968	10.2384
0.4	0.1	McGee <i>et al.</i> (1995)	48.6618	17.5822	9.3661	
		Zhou <i>et al.</i> (2009)	50.0059	17.7636	9.3961	
		Present ($N_r = N_z = 9$)	50.0045	17.7653	9.3945	
		Present ($N_r = N_z = 13$)	50.0059	17.7641	9.3958	
		Present ($N_r = N_z = 17$)	50.0056	17.7638	9.3961	
		Present ($N_r = N_z = 19$)	50.0056	17.7638	9.3962	
	210	0.2	McGee <i>et al.</i> (1995)	89.9678	20.9496	10.2631
			Zhou <i>et al.</i> (2009)	90.0265	20.9368	10.2418
			Present ($N_r = N_z = 9$)	90.0253	20.9347	10.2399
			Present ($N_r = N_z = 13$)	90.0260	20.9363	10.2410
			Present ($N_r = N_z = 17$)	90.0263	20.9369	10.2416
			Present ($N_r = N_z = 19$)	90.0264	20.9369	10.2416
270	0.1	McGee <i>et al.</i> (1995)	70.7344	19.6097	9.6643	
		Zhou <i>et al.</i> (2009)	71.8406	19.7064	9.6751	
		Present ($N_r = N_z = 9$)	71.8420	19.7040	9.6733	
		Present ($N_r = N_z = 13$)	71.8401	19.7059	9.6745	
		Present ($N_r = N_z = 17$)	71.8407	19.7063	9.6751	
		Present ($N_r = N_z = 19$)	71.8406	19.7063	9.6752	
	0.4	0.2	McGee <i>et al.</i> (1995)	48.6117	17.2943	8.8769
			Zhou <i>et al.</i> (2009)	49.9566	17.4733	8.9043
			Present ($N_r = N_z = 9$)	49.9535	17.4714	8.9026
			Present ($N_r = N_z = 13$)	49.9555	17.4725	8.9035
			Present ($N_r = N_z = 17$)	49.9563	17.4736	8.9041
			Present ($N_r = N_z = 19$)	49.9564	17.4735	8.9041
0.1	0.1	McGee <i>et al.</i> (1995)	89.6828	19.7282	8.5788	
		Zhou <i>et al.</i> (2009)	89.7655	19.7258	8.5635	
		Present ($N_r = N_z = 9$)	89.7634	19.7219	8.5611	
		Present ($N_r = N_z = 13$)	89.7642	19.7245	8.5623	
		Present ($N_r = N_z = 17$)	89.7651	19.7257	8.5630	
		Present ($N_r = N_z = 19$)	89.7653	19.7259	8.5633	
0.2	0.2	McGee <i>et al.</i> (1995)	70.5516	18.6218	8.1304	
		Zhou <i>et al.</i> (2009)	71.6588	18.7149	8.1386	
		Present ($N_r = N_z = 9$)	71.6551	18.7117	8.1365	

Table 2 Continued

α (deg)	h/a	Theories	C-C	F-C	F-S	
0.2		Present ($N_r = N_z = 13$)	71.6575	18.7139	8.1377	
		Present ($N_r = N_z = 17$)	71.6584	18.7150	8.1386	
		Present ($N_r = N_z = 19$)	71.6586	18.7150	8.1387	
	270	McGee <i>et al.</i> (1995)	48.4901	16.5657	7.5461	
		Zhou <i>et al.</i> (2009)	49.8361	16.7386	7.5670	
		Present ($N_r = N_z = 9$)	49.8341	16.7370	7.5650	
0.4		Present ($N_r = N_z = 13$)	49.8351	16.7382	7.5664	
		Present ($N_r = N_z = 17$)	90.0837	21.4263	10.8761	
		Present ($N_r = N_z = 19$)	90.1125	21.4074	10.8522	
	0.01	McGee <i>et al.</i> (1995)	90.1102	21.4065	10.8513	
		Zhou <i>et al.</i> (2009)	90.1124	21.4075	10.8520	
		Present ($N_r = N_z = 9$)	90.1122	21.4076	10.8525	
360		Present ($N_r = N_z = 13$)	90.1123	21.4076	10.8524	
		Present ($N_r = N_z = 17$)	70.8090	19.9986	10.2268	
		Present ($N_r = N_z = 19$)	71.9146	20.0967	10.2386	
	0.2	McGee <i>et al.</i> (1995)	71.9115	20.0954	10.2392	
		Zhou <i>et al.</i> (2009)	71.9142	20.0964	10.2380	
		Present ($N_r = N_z = 9$)	71.9143	20.0968	10.2385	
	0.4	Present ($N_r = N_z = 13$)	71.9143	20.0968	10.2384	
		Present ($N_r = N_z = 17$)	48.6618	17.5822	9.3661	
		Present ($N_r = N_z = 19$)	50.0059	17.7636	9.3961	
	0.01		McGee <i>et al.</i> (1995)	50.0045	17.7653	9.3945
			Zhou <i>et al.</i> (2009)	50.0059	17.7641	9.3958
			Present ($N_r = N_z = 9$)	50.0056	17.7638	9.3961
0.4		Present ($N_r = N_z = 13$)	50.0056	17.7638	9.3962	
		Present ($N_r = N_z = 17$)	89.9678	20.9496	10.2631	
		Present ($N_r = N_z = 19$)	90.0265	20.9368	10.2418	
0.01		Present ($N_r = N_z = 17$)	90.0253	20.9347	10.2399	

where $k = 1$ at $z = -0.5 h$ and $k = N_z$ at $z = 0.5 h$, and $j = 1, 2, \dots, N_r$. The boundary conditions at $r = b$ and a stated in (13)-(15) become,

Simply supported (S)

$$u_{zmk} = 0, \quad u_{\theta mjk} = 0,$$

$$(c_{11})_k \left(\sum_{n=1}^{N_r} A_{jn}^r u_{rmnk} \right) + (c_{12})_k \left(-\frac{m\pi}{r_j \alpha} u_{\theta mjk} + \frac{1}{r_j} u_{rmjk} \right) \quad (21a)$$

$$+ (c_{13})_k \left(\sum_{n=1}^{N_z} A_{kn}^z u_{zmjn} \right) = 0$$

Clamped (C)

$$u_{rmjk} = 0, u_{\theta mjk} = 0, u_{zmjk} = 0 \quad (21b)$$

Free (F)

$$(c_{11})_k \sum_{n=1}^{N_r} A_{jn}^r u_{rmnk} + (c_{12})_k \left(-\frac{m\pi}{r_j \alpha} u_{\theta mjk} + \frac{1}{r_j} u_{rmjk} \right) \quad (21c)$$

$$+ (c_{13})_k \sum_{n=1}^{N_z} A_{kn}^z u_{zmjn} = 0,$$

$$\sum_{n=1}^{N_r} A_{jn}^r u_{\theta mnk} + \frac{m\pi}{\alpha} u_{rmjk} - u_{\theta mjk} = 0, \quad (21c)$$

$$\sum_{n=1}^{N_z} A_{kn}^z u_{rmjn} + \sum_{n=1}^{N_r} A_{jn}^r u_{zmnk} = 0$$

In the above equations $k = 2, \dots, N_z - 1$; also $j = 1$ at $r = b$ and $j = N_r$ at $r = a$.

In order to carry out the eigenvalue analysis, the domain and boundary degrees of freedom are separated and in vector forms they are denoted as $\{d\}$ and $\{b\}$, respectively. Based on this definition, the discretized form of the equilibrium equations and the related boundary conditions take the following forms,

Equations of motion (17)-(19)

$$[[K_{db}][K_{dd}]] \begin{Bmatrix} \{b\} \\ \{d\} \end{Bmatrix} - \omega^2 [M] \{d\} = \{0\} \quad (22)$$

Boundary conditions (20) and (21a)-(21c)

$$[K_{bd}] \{d\} + [K_{bb}] \{b\} = \{0\} \quad (23)$$

Eliminating the boundary degrees of freedom in Eq. (22) using Eq.(23), this equation becomes

$$([K] - \omega^2 [M]) \{d\} = \{0\} \quad (24)$$

where $[K] = [K_{dd}] - [K_{db}][K_{bb}]^{-1}[K_{bd}]$. The above eigen value system of equations can be solved to find the natural frequencies of the sandwich plates.

4. Numerical results and discussion

In this section, the convergence behavior and accuracy of the method in evaluating the non-dimensional natural frequencies of isotropic and FGM annular sector plates with different set of boundary conditions along the circular edges are investigated.

McGee *et al.* (1995) provided the exact results for sector plates with a re-entrant corner, based on the Mindlin plate theory. As a first example, the comparative studies of the fundamental frequency parameters are given in Table 2. It is seen from Table 2 that for thin plates ($h/a = 0.01$) there is an excellent agreement between the present 3-D solutions and the classical solutions. For moderately thick plates ($h/a = 0.2$) the present 3-D solutions also agree quite well with the Mindlin solutions. For very thick plates ($h/a = 0.04$) the discrepancies increase, particularly for c-c plates. It is found that only nineteen DQ grid points in each direction (r and z) can yield accurate results. A numerical value of $N_r = N_z = 19$ is used for the next studies. The same problem has been analyzed by Zhou *et al.* (2009). It is obvious that the error of the Mindlin plate theory increases with the increase of the plate thickness, especially for very thick plates ($h/a \geq$

Table 3 The lowest non-dimensional frequency parameter ($\Omega = \omega h \sqrt{\rho/C_{11}}$) for FGMs annular sector plates having clamped ($r = b$) and clamped ($r = a$) conditions

α (deg)	h/a	b/a	m (circumferential wavenumber)	λ				
				1	2	3	4	5
195	0.1	1	Nie and Zhong (2008)	0.0663	0.0622	0.0566	0.0505	0.0446
			Present ($N_r = N_z = 9$)	0.0651	0.0611	0.0553	0.0497	0.0432
			Present ($N_r = N_z = 13$)	0.0661	0.0620	0.0561	0.0502	0.0440
			Present ($N_r = N_z = 17$)	0.0664	0.0622	0.0564	0.0505	0.0444
			Present ($N_r = N_z = 19$)	0.0664	0.0623	0.0564	0.0505	0.0445
		2	Nie and Zhong (2008)	0.0795	0.0746	0.0677	0.0603	0.0531
			Present ($N_r = N_z = 9$)	0.0781	0.0712	0.0666	0.0589	0.0519
			Present ($N_r = N_z = 13$)	0.0791	0.0743	0.0677	0.0601	0.0528
			Present ($N_r = N_z = 17$)	0.0793	0.0746	0.0679	0.0604	0.0530
			Present ($N_r = N_z = 19$)	0.0793	0.0747	0.0679	0.0603	0.0530
		0.3	Nie and Zhong (2008)	0.1041	0.0980	0.0895	0.0801	0.0710
			Present ($N_r = N_z = 9$)	0.1049	0.0968	0.0888	0.0789	0.0721
			Present ($N_r = N_z = 13$)	0.1041	0.0981	0.0896	0.0801	0.0712
			Present ($N_r = N_z = 17$)	0.1039	0.0979	0.0898	0.0799	0.0710
			Present ($N_r = N_z = 19$)	0.1039	0.0979	0.0897	0.0800	0.0710
	0.1	1	Nie and Zhong (2008)	0.1104	0.1039	0.0948	0.0849	0.0753
			Present ($N_r = N_z = 9$)	0.1094	0.1030	0.0933	0.0839	0.0741
			Present ($N_r = N_z = 13$)	0.1103	0.1038	0.0946	0.0845	0.0755
			Present ($N_r = N_z = 17$)	0.1106	0.1040	0.0950	0.0850	0.0751
			Present ($N_r = N_z = 19$)	0.1105	0.1039	0.0950	0.0850	0.0752
		2	Nie and Zhong (2008)	0.4040	0.3862	0.3611	0.3329	0.3046
			Present ($N_r = N_z = 9$)	0.4026	0.3842	0.3593	0.3314	0.3035
			Present ($N_r = N_z = 13$)	0.4038	0.3853	0.3604	0.3322	0.3045
			Present ($N_r = N_z = 17$)	0.4041	0.3863	0.3609	0.3326	0.3047
			Present ($N_r = N_z = 19$)	0.4041	0.3863	0.3610	0.3327	0.3048
		0.3	Nie and Zhong (2008)	0.5013	0.4781	0.4455	0.4091	0.3730
			Present ($N_r = N_z = 9$)	0.5001	0.4768	0.4438	0.4081	0.3719
			Present ($N_r = N_z = 13$)	0.5008	0.4764	0.4449	0.4090	0.3727
			Present ($N_r = N_z = 17$)	0.5011	0.4780	0.4453	0.4092	0.3730
			Present ($N_r = N_z = 19$)	0.5011	0.4779	0.4455	0.4092	0.3729
0.3	1	Nie and Zhong (2008)	0.5645	0.5436	0.5137	0.4796	0.4450	
		Present ($N_r = N_z = 9$)	0.5633	0.5425	0.5119	0.4776	0.4466	
		Present ($N_r = N_z = 13$)	0.5641	0.5440	0.5130	0.4790	0.4455	
		Present ($N_r = N_z = 17$)	0.5646	0.5436	0.5134	0.4794	0.4452	
		Present ($N_r = N_z = 19$)	0.5646	0.5435	0.5138	0.4796	0.4452	
	2	Nie and Zhong (2008)	0.6077	0.5840	0.5504	0.5125	0.4744	
		Present ($N_r = N_z = 9$)	0.6061	0.5852	0.5494	0.5120	0.4761	
		Present ($N_r = N_z = 13$)	0.6075	0.5846	0.5500	0.5127	0.4754	
		Present ($N_r = N_z = 17$)	0.6079	0.5843	0.5505	0.5124	0.4748	
		Present ($N_r = N_z = 19$)	0.6079	0.5842	0.5505	0.5124	0.4746	
	0.1	Nie and Zhong (2008)	0.0659	0.0619	0.0563	0.0502	0.0443	
		Present ($N_r = N_z = 9$)	0.0651	0.0603	0.0550	0.0509	0.0451	
		Present ($N_r = N_z = 13$)	0.0665	0.0617	0.0555	0.0504	0.0440	
		Present ($N_r = N_z = 17$)	0.0661	0.0621	0.0560	0.0501	0.0445	
		Present ($N_r = N_z = 19$)	0.0660	0.0621	0.0561	0.0501	0.0444	

Table 3 Continued

α (deg)	h/a	b/a	m (circumferential wavenumber)	λ					
				1	2	3	4	5	
210	0.1	0.1	2	Nie and Zhong (2008)	0.0766	0.0719	0.0653	0.0581	0.0512
				Present ($N_r = N_z = 9$)	0.0751	0.0705	0.0641	0.0573	0.0500
				Present ($N_r = N_z = 13$)	0.0760	0.0717	0.0650	0.0581	0.0508
				Present ($N_r = N_z = 17$)	0.0765	0.0720	0.0655	0.0583	0.0511
				Present ($N_r = N_z = 19$)	0.0765	0.0721	0.0654	0.0583	0.0510
				Nie and Zhong (2008)	0.1039	0.0978	0.0892	0.0799	0.0708
		Present ($N_r = N_z = 9$)	0.1025	0.0969	0.0883	0.0787	0.0681		
		Present ($N_r = N_z = 13$)	0.1033	0.0979	0.0892	0.0807	0.0693		
		Present ($N_r = N_z = 17$)	0.1038	0.0976	0.0895	0.0801	0.0701		
		Present ($N_r = N_z = 19$)	0.1037	0.0977	0.0895	0.0800	0.0706		
		Present ($N_r = N_z = 13$)	0.1095	0.1033	0.0939	0.0842	0.0749		
		Present ($N_r = N_z = 17$)	0.1091	0.1028	0.0936	0.0839	0.0744		
	Present ($N_r = N_z = 19$)	0.1092	0.1029	0.0935	0.0839	0.0745			
	0.3	0.1	1	Nie and Zhong (2008)	0.4002	0.3827	0.3580	0.3302	0.3023
				Present ($N_r = N_z = 9$)	0.4018	0.3815	0.3598	0.3318	0.3003
				Present ($N_r = N_z = 13$)	0.4007	0.3824	0.3587	0.3308	0.3018
				Present ($N_r = N_z = 17$)	0.4001	0.3829	0.3581	0.3303	0.3023
				Present ($N_r = N_z = 19$)	0.4000	0.3829	0.3582	0.3304	0.3023
				Nie and Zhong (2008)	0.4832	0.4608	0.4294	0.3943	0.3594
		Present ($N_r = N_z = 9$)	0.4813	0.4622	0.4277	0.3931	0.3577		
		Present ($N_r = N_z = 13$)	0.4826	0.4611	0.4288	0.3940	0.3587		
		Present ($N_r = N_z = 17$)	0.4834	0.4605	0.4295	0.3944	0.3594		
		Present ($N_r = N_z = 19$)	0.4833	0.4606	0.4296	0.3944	0.3595		
		0.3	0.1	2	Nie and Zhong (2008)	0.5630	0.5421	0.5123	0.4784
Present ($N_r = N_z = 9$)					0.5618	0.5404	0.5105	0.4799	0.4424
Present ($N_r = N_z = 13$)	0.5629				0.5415	0.5117	0.4790	0.4434	
Present ($N_r = N_z = 17$)	0.5633				0.5422	0.5121	0.4785	0.4439	
Present ($N_r = N_z = 19$)	0.5633				0.5421	0.5121	0.4784	0.4440	
Nie and Zhong (2008)	0.5990				0.5756	0.5428	0.5056	0.4682	
Present ($N_r = N_z = 9$)	0.5977		0.5771	0.5441	0.5041	0.4702			
Present ($N_r = N_z = 13$)	0.5984		0.5760	0.5433	0.5050	0.4690			
Present ($N_r = N_z = 17$)	0.5990		0.5756	0.5429	0.5055	0.4683			
Present ($N_r = N_z = 19$)	0.5991		0.5755	0.5429	0.5057	0.4683			

0.4). The two-dimensional theories, such as the classical plate theory, the first and the higher order shear deformation plate theories neglect transverse normal deformations, and generally assume that a plane stress state of deformation prevails in the plate. These assumptions may be appropriate for thin plates but do not give good results for thick plates. It is seen from Table 2 that the maximum differences between the 3-D solutions and the Mindlin solutions occur at the clamped-clamped plates. As the second example, the convergence behavior and accuracy of the method for lowest non-dimensional frequency parameter ($\omega =$

$\omega h \sqrt{\rho/C_{11}}$) of thick FG annular sector plates with clamped-clamped boundary condition at circular edges is studied in Table 3. The results are compared with those of the three-dimensional elasticity solutions of Nie and Zhong (2008) which were obtained using the State space method (S.S.M). It is assumed that the material properties vary exponentially $\left(c_{ij}(z) = c_{ij}^M e^{\left(\frac{\lambda z}{h}\right)}, \rho(z) = \rho^M e^{\left(\frac{\lambda z}{h}\right)} \right)$ through the thickness of the plate. Superscripts M denote the material properties of the bottom surface of the plate, λ is the

material property graded index. One can see that an excellent agreement exists between the converged results of the presented approach and the other one.

In this section, we characterize the response of FG-MWCNT sandwich plate with graded reinforcement volume fractions in the plate's thickness. The non-dimensional natural frequency is as follows

$$\Omega = \alpha \alpha^2 \sqrt{\rho_i h / D_i}, \quad D_i = E_i h^3 / 12(1 - \nu_i^2) \quad (25)$$

where ρ_i, E_i and ν_i are mechanical properties of MWCNTs.

Fig. 4 and Tables 4 and 5 show the influence of the constituent volume fractions “ p ” on the first two non-dimensional natural frequencies of the FG-MWCNTs

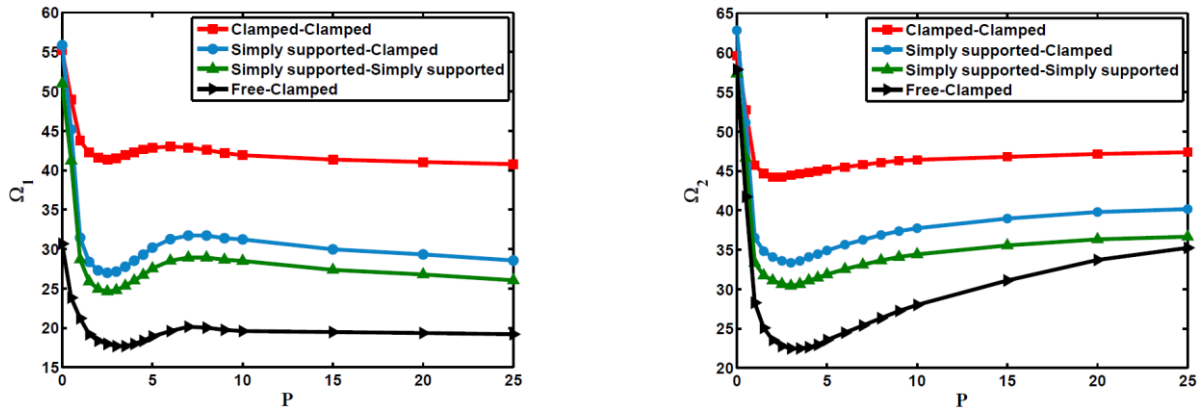


Fig. 4 Variation of the first and second non-dimensional natural frequency parameter of FG-MWCNTs sandwich plates versus “ p ” ($h/a = 0.2, b/a = 0/2, \alpha = 195^\circ$)

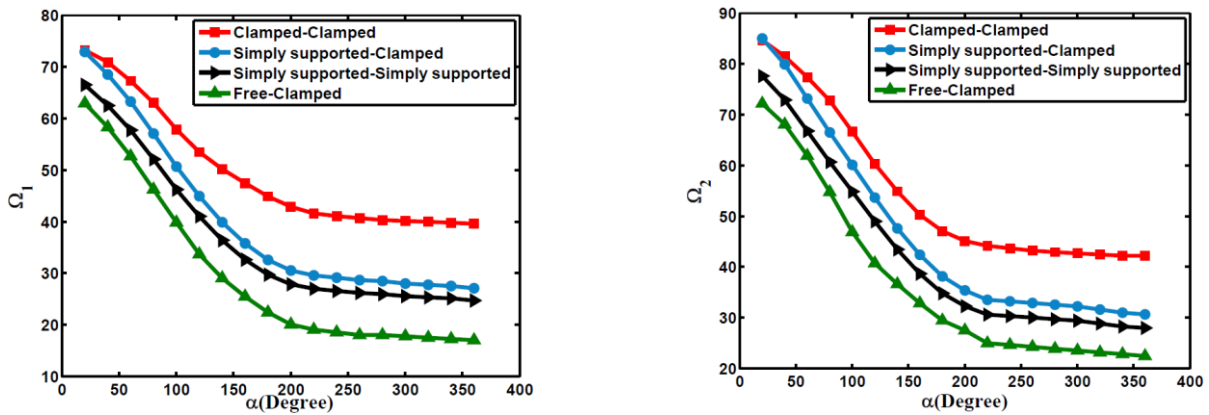


Fig. 5 The influence of the sector angle on the first and second non-dimensional natural frequency parameter of FG-MWCNTs sandwich plates ($b/a = h/a = 0/2, p = 1$)

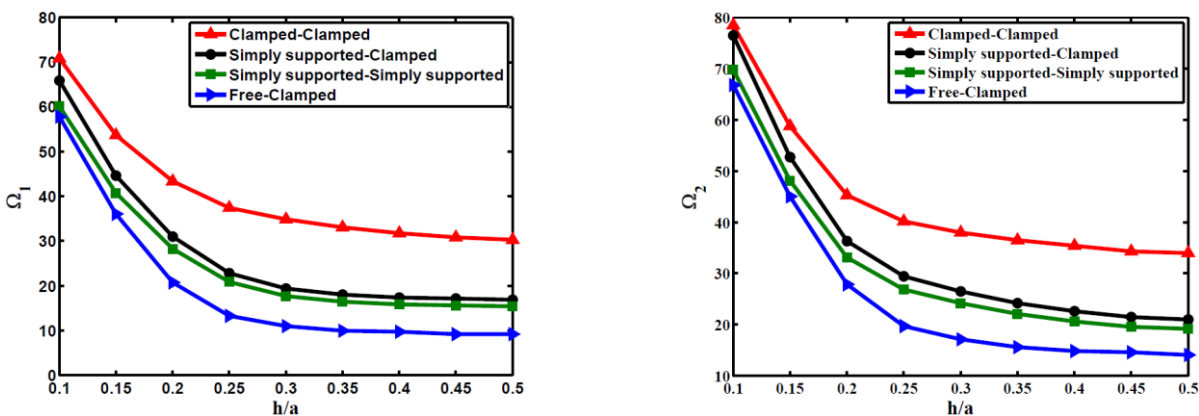


Fig. 6 Variation of the first and second non-dimensional natural frequency parameter of FG-MWCNTs sandwich plates versus h/a ($b/a = 0.2, p = 1, \alpha = 195^\circ$)

Table 4 The effect of exponent parameter (p) on the first non-dimensional natural frequency parameter of sandwich sectorial plate with MWCNT core ($h/a = b/a = 0.2, \alpha = 195^\circ$)

Exponent parameter (p)	C-C	S-C	S-S	F-C
0	55.2328	55.8419	50.9614	30.6560
1	43.7386	31.4231	28.6768	21.0010
5	42.8250	30.1736	27.5365	18.9202
10	41.8943	31.2161	28.4878	19.6124
15	41.3404	29.9666	27.3475	19.4640
20	41.0149	29.3240	26.7611	19.3280
25	40.7408	28.5314	26.0378	19.1920

Table 5 The effect of exponent parameter (p) on the second non-dimensional natural frequency parameter of sandwich sectorial plate with MWCNT core ($h/a = b/a = 0.2, \alpha = 195^\circ$)

Exponent parameter (p)	C-C	S-C	S-S	F-C
0	59.6124	62.7963	57.3079	57.8480
1	45.7028	36.5068	33.3161	28.2560
5	45.1718	34.4219	31.8565	23.5360
10	46.4109	37.7063	34.4108	28.0025
15	46.7706	38.9273	35.5250	31.0800
20	47.1361	39.7769	36.3004	33.6960
25	47.3587	40.1482	36.6393	35.2320

Table 6 The effect of sector angle (α) on the first non-dimensional natural frequency parameter of sandwich sectorial plate with MWCNT core ($p = 1, h/a = b/a = 0.2$)

α (deg)	C-C	S-C	S-S	F-C
0	59.6124	62.7963	57.3079	57.8480
1	45.7028	36.5068	33.3161	28.2560
5	45.1718	34.4219	31.8565	23.5360
10	46.4109	37.7063	34.4108	28.0025
15	46.7706	38.9273	35.5250	31.0800
20	47.1361	39.7769	36.3004	33.6960
25	47.3587	40.1482	36.6393	35.2320

sandwich sector plates with different types of boundary condition.

It is observed with increasing power-law exponent " p " the first two non-dimensional natural frequencies decrease sharply for small value of " p " ($p < 1$) and then for $p > 15$ it reaches a constant value for different types of boundary condition. It should be noted that second derivative of the curves in Fig. 3 is positive for $p < 1$ and negative for $p > 1$. It is obvious for $p = 1$, the second derivative is equal to zero. Therefore, in Fig. 4 the curves have a first decreasing branch, followed by an increasing part, and finally they become constant for $p > 15$, because the volume fraction of

Table 7 The effect of sector angle (α) on the second non-dimensional natural frequency parameter of sandwich sectorial plate with MWCNT core ($p = 1, h/a = b/a = 0.2$)

α (deg)	C-C	S-C	S-S	F-C
20	84.6793	85.0374	77.6051	72.1680
60	77.3705	73.1850	66.7886	61.9200
100	66.6357	60.0902	54.8384	46.8960
140	54.9017	47.5952	43.4354	36.6480
200	45.1433	35.3858	32.2931	27.5120
240	43.6815	33.2224	30.3188	24.6320
300	42.7051	32.2585	29.4391	23.5520

Table 8 The effect of thickness-to-outer radius ratio (h/a) on the first non-dimensional natural frequency parameter of sandwich sectorial plate with MWCNT core ($b/a = 0.2, p = 1, \alpha = 195^\circ$)

h/a	C-C	S-C	S-S	F-C
0.1	70.8611	65.8808	60.1228	57.8240
0.15	53.6911	44.6393	40.7378	36.0800
0.2	43.7386	31.4231	28.6768	21.0010
0.25	37.4405	22.8337	20.8381	13.3040
0.3	34.8824	19.4137	17.7169	11.0011
0.35	33.0552	18.0428	16.4658	9.9760
0.1	70.8611	65.8808	60.1228	57.8240

Table 9 The effect of thickness-to-outer radius ratio (h/a) on the second non-dimensional natural frequency parameter of sandwich sectorial plate with MWCNT core ($b/a = 0.2, p = 1, \alpha = 195^\circ$)

h/a	C-C	S-C	S-S	F-C
0.1	78.5125	76.4694	69.7860	66.7840
0.15	58.8130	52.7503	48.1399	45.0320
0.2	45.7028	36.5068	33.3161	28.2560
0.25	40.1756	29.4596	26.8849	19.7040
0.3	37.9829	26.4894	24.1742	17.1440
0.35	36.5269	24.2046	22.0891	15.6080
0.1	78.5125	76.4694	69.7860	66.7840

the reinforcement gets approximately constant along the thickness of the plate.

The influences of the sector angle on the fundamental frequency parameter of FG-MWCNTs sandwich sector plates with different circular edge conditions are shown in Fig. 5 and also in Tables 6 and 7. It is obvious that by increasing the sector angle, the frequency parameter decreases. The variation of h/a ratio with the frequency parameters of Clamped-Clamped, Simply Supported-Clamped, Simply Supported-Simply Supported and Free-Clamped FG-MWCNTs sandwich annular sector plates are shown in Fig. 6 and also in Tables 8 and 9. It is observed that for both first and second frequency parameters and for different boundary conditions, the frequency parameter

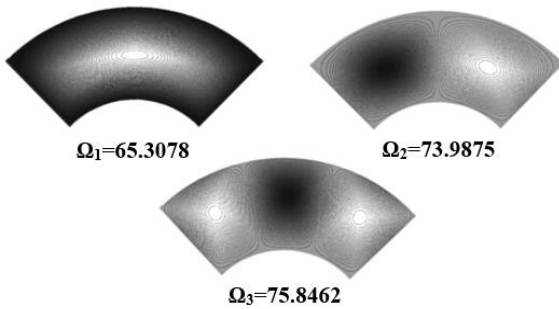


Fig. 7 Mode shape plots of annular sandwich sector plates with Clamped-Clamped boundary conditions at the circular edges ($h/a = b/a = 0.2$, $\alpha = 90^\circ$, $p = 1$)

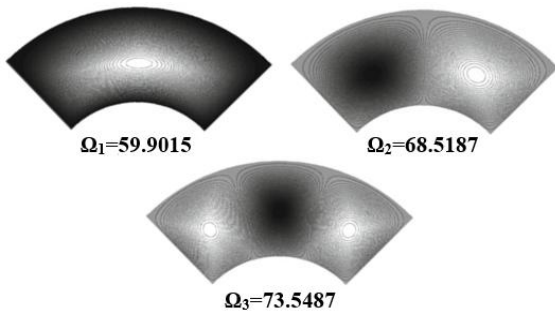


Fig. 8 Mode shape plots of annular sandwich sector plates with Simply Supported-Clamped boundary conditions at the circular edges ($h/a = b/a = 0.2$, $\alpha = 90^\circ$, $p = 1$)

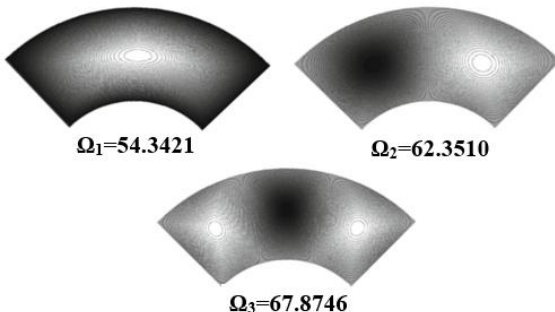


Fig. 9 Mode shape plots of annular sandwich sector plates with Simply Supported-Simply Supported boundary conditions at the circular edges ($h/a = b/a = 0.2$, $\alpha = 90^\circ$, $p = 1$)

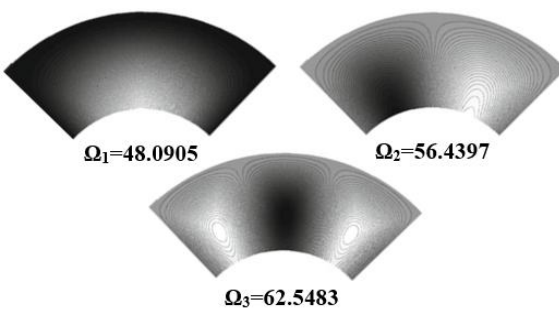


Fig. 10 Mode shape plots of annular sandwich sector plates with Free-Clamped boundary conditions at the circular edges ($h/a = b/a = 0.2$, $\alpha = 90^\circ$, $p = 1$)

increases with the increase of h/a ratio and then it becomes unaltered for great amounts of thickness-to-outer radius ratio.

It is observed that (Tables 4-9) with increasing the rigidity of the structure the frequency parameter increases.

For an overall comprehension on 3-D vibration of annular sector plates, some mode shape contour plots for different types of boundary conditions are depicted in Figs. 7-10.

5. Conclusions

In this research work, free vibration of functionally graded multi-walled carbon nanotubes sandwich annular sector plates is investigated based on three-dimensional theory of elasticity. Three complicated equations of motion for the plate under consideration are semi-analytically solved by using 2-D differential quadrature method. Using the 2-D differential quadrature method in the r - and z -directions, allows one to deal with FG plates with arbitrary thickness distribution of material properties and also to implement the effects of boundary conditions at the circular edges of the plate efficiently and in an exact manner. The fast rate of convergence and accuracy of the method are investigated through the different solved examples. The effects of different geometrical parameters such as the thickness-to-outer radius ratio and boundary conditions on the performance of the natural frequency parameters of FG-MWCNT sandwich plates are investigated. Modified Halpin-Tasi equation is used to evaluate the Young's modulus of the MWCNT/epoxy composite samples by the incorporation of an orientation as well as an exponential shape factor in the equation. The exponential shape factor modifies the Halpin-Tsai equation from expressing a straight line to a nonlinear one in the MWNTs wt% range considered.

The main contribution of this work is to present useful results for continuous grading of MWCNT reinforcement in the thickness direction of the plate. From this study some conclusions can be made as following:

- It is observed with increasing power-law exponent " p " the first two non-dimensional natural frequencies decrease sharply for small value of " p " ($p < 1$) and then for $p > 15$ it reaches a constant value for different types of boundary condition. It should be noted that second derivative of the curves in Fig. 3 is positive for $p < 1$ and negative for $p > 1$. It is obvious for $p = 1$, the second derivative is equal to zero. Therefore, in Fig. 4 the curves have a first decreasing branch, followed by an increasing part, and finally they become constant for $p > 15$, because the volume fraction of the reinforcement gets approximately constant along the thickness of the plate.
- It is obvious that by increasing the sector angle, the frequency parameter decreases.

Results show that for both first and second frequency parameters and for different boundary conditions, the

frequency parameter increases with the increase of h/a ratio and then it becomes unaltered for great amounts of thickness-to-outer radius ratio.

References

- Affdl Halpin, J.C. and Kardos, J.L. (1976), "The Halpin-Tsai equations: A review", *Polym. Eng. Sci.*, **16**(5), 344-352.
- Arefi, M. (2015), "Elastic solution of a curved beam made of functionally graded materials with different cross sections", *Steel Compos. Struct., Int. J.*, **18**(3), 659-672.
- Anderson, T.A. (2003), "A 3-D elasticity solution for a sandwich composite with functionally graded core subjected to transverse loading by a rigid sphere", *Compos. Struct.*, **60**(3), 265-274.
- Bapu Rao, M.N., Guruswamy, P. and Sampath Kumaran, K.S. (1977), "Finite element analysis of thick annular and sector plates", *Nucl. Eng. Des.*, **41**(2), 247-255.
- Barka, M., Benrahou, K.H., Bakora, A. and Tounsi, A. (2016), "Thermal post-buckling behavior of imperfect temperature-dependent sandwich FGM plates resting on Pasternak elastic foundation", *Steel Compos. Struct., Int. J.*, **22**(1), 91-112.
- Bennai, R., Ait Atmane, H. and Tounsi, A. (2015), "A new higher-order shear and normal deformation theory for functionally graded sandwich beams", *Steel Compos. Struct., Int. J.*, **19**(3), 521-546.
- Benson, P.R. and Hinton, E. (1976), "A thick finite strip solution for static, free vibration and stability problems", *Int. J. for Numer. Methods Eng.*, **10**(3), 665-678.
- Bert, C.W. and Malik, M. (1996), "Differential quadrature method in computational mechanics: A review", *Appl. Mech. Rev.*, **49**(1), 1-27.
- Bouchafa, A., Bouiadjra, M.B., Houari, M.S.A. and Tounsi, A. (2015), "Thermal stresses and deflections of functionally graded sandwich plates using a new refined hyperbolic shear deformation theory", *Steel Compos. Struct., Int. J.*, **18**(6), 1493-1515.
- Bouguenina, O., Belakhdar, K., Tounsi, A. and Bedia, E.A.A. (2015), "Numerical analysis of FGM plates with variable thickness subjected to thermal buckling", *Steel Compos. Struct., Int. J.*, **19**(3), 679-695.
- Chen, C.S., Liu, F.H. and Chen, W.R. (2017), "vibration and stability of initially stressed sandwich plates with FGM face sheets in thermal environments", *Steel Compos. Struct., Int. J.*, **23**(3), 251-261.
- Cheung, M.S. and Chan, M.Y.T. (1981), "Static and dynamic analysis of thin and thick sectorial plates by the finite strip method", *Comput. Struct.*, **14**(1-2), 79-88.
- Fidelus, J.D., Wiesel, E., Gojny, F.H., Schulte, K. and Wagner, H.D. (2005), "Thermo-mechanical properties of randomly oriented carbon/epoxy nanocomposites", *Composites Part A*, **36**(11), 1555-1561.
- Finot, M. and Suresh, S. (1996), "Small and large deformation of thick and thin-film multilayers: Effect of layer geometry, plasticity and compositional gradients", *J. Mech. Phys. Solids*, **44**(5), 683-721.
- Ghavamian, A., Rahmandoust, M. and Öchsner, A. (2012), "A numerical evaluation of the influence of defects on the elastic modulus of single and multi-walled carbon nanotubes", *Comput. Mater. Sci.*, **62**, 110-116.
- Gojny, F.H., Wichmann, M.H.G., Fiedler, B. and Schulte, K. (2005), "Influence of different carbon nanotubes on the mechanical properties of epoxy matrix composites-A comparative study", *Compos. Sci. Technol.*, **65**(15-16), 2300-2313.
- Guruswamy, P. and Yang, T.Y. (1979), "A sector finite element for dynamic analysis of thick plates", *J. Sound Vib.*, **62**(4), 505-516.
- Halpin, J.C. and Tsai, S.W. (1969), "Effects of environmental factors on composite materials", *AFML-TR-67-423*.
- Houmat, A. (2001), "A sector Fourier p-element applied to free vibration analysis of sectorial plates", *J. Sound Vib.*, **243**(2), 269-282.
- Kamarian, S., Yas, M.H. and Pourasghar, A. (2013), "Free vibration analysis of three-parameter functionally graded material sandwich plates resting on Pasternak foundations", *J. Sandw. Struct. Mater.*, **15**(3), 292-308.
- Kashtalyan, M. and Menshykova, M. (2009), "Three-dimensional elasticity solution for sandwich panels with a functionally graded core", *Compos. Struct.*, **87**(1), 36-43.
- Kim, C.S. and Dickinson, S.M. (1989), "On the free, transverse vibration of annular and circular, thin, sectorial plates subjected to certain complicating effects", *J. Sound Vib.*, **134**(3), 407-421.
- Koizumi, M. (1993), "The concept of FGM", *Ceram. Trans. Funct. Grad. Mater.*, **34**, 3-10.
- Leissa, A.W., McGee, O.G. and Huang, C.S. (1993), "Vibrations of sectorial plates having corner stress singularities", *J. Appl. Mech. Transactions of the ASME*, **60**(1), 134-140.
- Li, Q., Iu, V. and Kou, K. (2008), "Three-dimensional vibration analysis of functionally graded material sandwich plates", *J. Sound Vib.*, **311**(1-2), 498-515.
- Liew, K.M. and Lam, K.Y. (1993), "On the use of 2-d orthogonal polynomials in the Rayleigh-Ritz method for flexural vibration of annular sector plates of arbitrary shape", *Int. J. Mech. Sci.*, **35**(2), 129-139.
- Liew, K.M. and Liu, F.L. (2000), "Differential quadrature method for vibration analysis of shear deformable annular sector plates", *J. Sound Vib.*, **230**(2), 335-356.
- Marin, M. (1997), "On weak solutions in elasticity of dipolar bodies with voids", *J. Compos. Appl. Math.*, **82**(1-2), 291-297.
- Marin, M. (2010a), "A domain of influence theorem for microstretch elastic materials", *Nonlinear Anal. Real World Appl.*, **11**(5), 3446-3452.
- Marin, M. (2010b), "Harmonic vibrations in thermoelasticity of microstretch materials", *J. Vib. Acoust. ASME*, **132**(4), 044501-1_044501-6.
- Marin, M. (1994), "The Lagrange identity method in thermoelasticity of bodies with microstructure", *Int. J. Eng. Sci.*, **32**(8), 1229-1240.
- Martone, A., Faiella, G., Antonucci, V., Giordano, M. and Zarrelli, M. (2011), "The effect of the aspect ratio of carbon nanotubes on their effective reinforcement modulus in an epoxy matrix", *Compos. Sci. Technol.*, **71**(8), 1117-1123.
- McGee, O.G., Huang, C.S. and Leissa, A.W. (1995), "Comprehensive exact solutions for free vibrations of thick annular sectorial plates with simply supported radial edges", *Int. J. Mech. Sci.*, **37**(5), 537-566.
- Mizusawa, T. (1991), "Vibration of thick annular sector plates using semi-analytical methods", *J. Sound Vib.*, **150**(2), 245-259.
- Montazeri, A., Javadpour, J., Khavandi, A., Tcharkhtchi, A. and Mohajeri, A. (2010), "Mechanical properties of multi-walled carbon nanotube/epoxy composites", *Mater. Des.*, **31**(9), 4202-4208.
- Moradi-Dastjerdi, R. and Momeni-Khabisi, H. (2016), "Dynamic analysis of functionally graded nanocomposite plates reinforced by wavy carbon nanotube", *Steel Compos. Struct., Int. J.*, **22**(2), 277-299.
- Mukhopadhyay, M. (1979), "A semi-analytic solution for free vibration of annular sector plates", *J. Sound Vib.*, **63**(1), 87-95.
- Mukhopadhyay, M. (1982), "Free vibration of annular sector plates with edges possessing different degrees of rotational restraints", *J. Sound Vib.*, **80**(2), 275-279.
- Nie, G.J. and Zhong, Z. (2008), "Vibration analysis of functionally graded annular sectorial plates with simply supported radial

- edges”, *Compos. Struct.*, **84**(2), 167-176.
- Park, W.T., Han, S.C., Jung, W.Y. and Lee, W.H. (2016), “Dynamic instability analysis for S-FGM plates embedded in Pasternak elastic medium using the modified couple stress theory”, *Steel Compos. Struct., Int. J.*, **22**(6), 1239-1259.
- Pelletier Jacob, L. and VelSenthil, S. (2006), “An exact solution for the steady state thermo elastic response of functionally graded orthotropic cylindrical shells”, *Int. J. Solid Struct.*, **43**(5), 1131-1158.
- Ramaiah, G.K. and Vijayakumar, K. (1974), “Natural frequencies of circumferentially truncated sector plates with simply supported straight edges”, *J. Sound Vib.*, **34**(1), 53-61.
- Ramakris, R. and Kunukkas, V.X. (1973), “Free vibration of annular sector plates”, *J. Sound Vib.*, **30**(1), 127-129.
- Reddy, J.N. (2013), *An Introduction to Continuum Mechanics*, (2nd Edition), Cambridge University Press.
- Seok, J.W. and Tiersten, H.F. (2004), “Free vibrations of annular sector cantilever plates part 1: out-of-plane motion”, *J. Sound Vib.*, **271**(3-5), 757-772.
- Sharma, K. and Marin, M. (2013), “Effect of distinct conductive an thermodynamic temperatures on the reflection of plane waves in micropolar elastic half-space”, *U.P.B. Sci. Bull., Series A-Appl. Math. Phys.*, **75**(2), 121-132.
- Sharma, A., Sharda, H.B. and Nath, Y. (2005a), “Stability and vibration of Mindlin sector plates: An analytical approach”, *AIAA Journal*, **43**(5), 1109-1116.
- Sharma, A., Sharda, H.B. and Nath, Y. (2005b), “Stability and vibration of thick laminated composite sector plates”, *J. Sound Vib.*, **287**(1-2), 1-23.
- Srinivasan, R.S. and Thiruvengkatachari, V. (1983), “Free vibration of annular sector plates by an integral equation technique”, *J. Sound Vib.*, **89**(3), 425-432.
- Srinivasan, R.S. and Thiruvengkatachari, V. (1986), “Free vibration analysis of laminated annular sector plates”, *J. Sound Vib.*, **109**(1), 89-96.
- Swaminadham, M., Danielski, J. and Mahrenholtz, O. (1984), “Free vibration analysis of annular sector plates by holographic experiments”, *J. Sound Vib.*, **95**(3), 333-340.
- Tahouneh, V. (2016), “Using an equivalent continuum model for 3D dynamic analysis of nanocomposite plates”, *Steel Compos. Struct., Int. J.*, **20**(3), 623-649.
- Tahouneh, V. and Naei, M.H. (2016), “Free vibration and vibrational displacements analysis of thick elastically supported laminated curved panels with power-law distribution functionally graded layers and finite length via 2D GDQ method”, *J. Sandw. Struct. Mater.*, **18**(3), 263-293.
- Wagner, H.D., Lourie, O. and Feldman, Y. (1997), “Stress-induced fragmentation of multiwall carbon nanotubes in a polymer matrix”, *Appl. Phys. Lett.*, **72**(2), 188-190.
- Wang, Z.X. and Shen, H.S. (2011), “Nonlinear vibration and bending of sandwich plates with nanotube-reinforced composite face sheets”, *Compos. Part B*, **43**(2), 411-421.
- Wu, C.P. and Liu, Y.C. (2016), “A state space meshless method for the 3D analysis of FGM axisymmetric circular plates”, *Steel Compos. Struct., Int. J.*, **22**(1), 161-182.
- Xiang, Y., Liew, K.M. and Kitipornchai, S. (1993), “Transverse vibration of thick annular sector plates”, *J. Eng. Mech. ASCE*, **119**(8), 1579-1599.
- Yeh, M.K., Tai, N.H. and Liu, J.H. (2006), “Mechanical behavior of phenolic-based composites reinforced with multi-walled carbon nanotubes”, *Carbon*, **44**(1), 1-9.
- Zenkour, A. (2005a), “A comprehensive analysis of functionally graded sandwich plates, Part 1-Deflection and stresses”, *Int. J. Solids Struct.*, **42**(18-19), 5224-5242.
- Zenkour, A. (2005b), “A comprehensive analysis of functionally graded sandwich plates: Part 2-Buckling and free vibration”, *Int. J. Solids Struct.*, **42**(18-19), 5243-5258.
- Zhou, D., Lo, S.H. and Cheung, Y.K. (2009), “3-D vibration analysis of annular sector plates using the Chebyshev-Ritz method”, *J. Sound Vib.*, **320**(1-2), 421-437.
- Zhu, X.H. and Meng, Z.Y. (1995), “Operational principle fabrication and displacement characteristics of a functionally gradient piezoelectric ceramic actuator”, *Sens. Actuators*, **48**(3), 169-176.

CC